Snowmelt Dynamics in a Temperate Glacier Using Sentinel-1 SAR Images: A Case Study on Saint-Sorlin Glacier, French Alps

Clémence Turbé, Fatima Karbou, Antoine Rabatel, Isabelle Gouttevin

Snowmelt Dynamics in a Temperate Glacier Using Sentinel-1 SAR Images: A Case Study on Saint-Sorlin Glacier, French Alps

Clémence Turbé, Fatima Karbou, Antoine Rabatel, and Isabelle Gouttevin

***Abstract*—Snow and glaciers play a crucial role in various applications such as hydrology, climate, and avalanche risk assessment. Remote sensing is a powerful tool for monitoring the snowpack and melt in glacier catchments. Synthetic aperture radar (SAR) imagery, which measures the backscattering signal in the microwave spectrum, is particularly useful for studying snow and glacier-related issues. While it is almost insensitive to cloud cover, it is sensitive to some snow/glacier properties such as liquid water content. In this study, we analyze the snowmelt dynamics in the Saint-Sorlin Glacier catchment in the French Alps using SAR images in *C*-band from Sentinel-1. Our primary objective is to understand the spatial and temporal variabilities of the SAR signal in a glacierized area by monitoring the SAR signal in regions of snow/ice ablation, accumulation, and outside the glacier. We also rely on complementary meteorological, model, and optical data. A second objective is to compare and assess several approaches from the literature to characterize the snowmelt dynamics on a variety of surfaces. Our study confirms and extends the capability of previous methodologies to identify crucial melting phases, such as moistening of the snowpack, saturation, and run-off phases, using SAR backscatter time series. These melting phases were compared with the ones estimated from liquid water content and snow water equivalent simulations simulated with the Crocus state-of-the-art snowpack model. The transition from snow-covered to an icy surface on ablation areas was detected using VH-polarized images, as SAR imagery is sensitive to surface roughness.**

***Index Terms*—French Alps, glacierized catchment, glaciers, Sentinel-1, snow melt dynamics, synthetic aperture radar (SAR) imagery, total snow, wet snow.**

I. Introduction

CLIMATE change has a significant impact on the evolution of glaciers over time. The mass gain or loss of glaciers depends on the balance between snow supply in the accumulation zone and melting in the ablation zone [1]. Therefore, the dynamics of glaciers are influenced by meteorological variables (e.g., temperature, precipitation, and solar radiation), glacier flow processes, and topographical conditions [2], [3]. With the ever-increasing impact of climate change, mountain glaciers are a major source of risk not only in their vicinity but also for the communities downstream [4]. More specifically, the retreat of several alpine glaciers [5], [6] amplifies risks such as falling seracs, outbursts of glacial lakes, or englacial water pockets [7], [8]. The consequences of these risks are not only environmental but also socio-economic [4]. Managing and preventing glacier-related risks requires both a thorough understanding of glacier dynamics and the capability to effectively monitor critical variables such as glacier length, surface area, and thickness, as well as surface flow velocity and mass balance [9].

Among them, the elevation of the snow line, which marks the boundary between snow and ice, is an essential variable in hydrology and glaciology. In alpine regions, it is related to the amount of seasonal melt, and correlates with the surface mass balance of the glacier. Above the snow line, the extent of the accumulation area controls the amount of ice formation. The snow line at the end of the ablation season is a good proxy of the equilibrium-line altitude (ELA) for temperate glaciers [10]. Therefore, remote sensing applications use this assumption to infer glacier-wide mass balance from optical satellite images and digital elevation model (DEM) [11], [12].

Measuring and monitoring variables related to glacier behaviors can be complex without satellite data, as most of these high-altitude areas are remote and inaccessible, and lead to scarce *in situ* observations. It is therefore common to use optical sensors like SPOT, Pléiades, Sentinel-2, Landsat, and ASTER, which can monitor snow, glacier ice, and other hydrological variables [12], [13], [14], [15], [16]. Optical imagery are also able to distinguish snow and firn from glacier ice: for instance, Paul et al. [17] used a false color composite with Sentinel-2 spectral bands. However, using these sensors can be challenging in alpine regions due to cloud cover and shadow issues. As an alternative, active microwave data from synthetic aperture radar (SAR) can be an excellent option to monitor glaciers since it is almost insensitive to weather conditions or time of day [18]. Additionally, SAR imagery has the advantage of being sensitive to liquid water content due to the strong dielectric contrast between the wet and dry ground surfaces [19]. However, due to geometric distortion issues, these data can also be quite complex to use in mountainous areas [20]. In recent years, SAR intensity images from Sentinel-1 have been extensively used to identify

Manuscript received 5 December 2023; revised 29 February 2024; accepted 25 March 2024. Date of publication 1 April 2024; date of current version 1 May 2024. *(Corresponding author: Clémence Turbé.)*

Clémence Turbé, Fatima Karbou, and Isabelle Gouttevin are with the Université Grenoble Alpes, 38400 Saint-Martin-d'Hères, France, also with the Université de Toulouse, Météo-France, 38400 Saint-Martin-d'Hères, France, and also with the CNRS, CNRM, Centre d'Études de la Neige, 38000 Grenoble, France (e-mail: clemence.turbe@meteo.fr).

Antoine Rabatel is with the Université Grenoble Alpes, 38400 Saint-Martin-d'Hères, France, and also with the CNRS, IRD, INRAE, Grenoble-INP, Institut des Géosciences de l'Environnement (IGE, UMR5001), 38000 Grenoble, France.

Digital Object Identifier 10.1109/JSTARS.2024.3384030

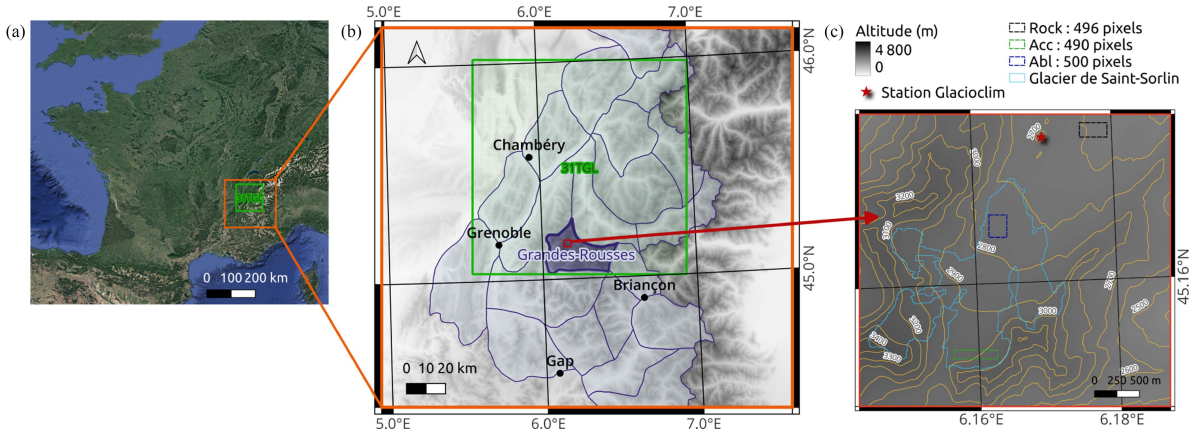

Fig. 1. Location of the study area. (a) Outline of the 31TGL tile (in green). (b) Zoom into the orange square of (a); outlines of the different massifs in the French Alps (blue outline). Saint-Sorlin Glacier is located in the Grandes-Rousses massif (dark blue outline). (c) Zoom into the red square of (b); the light blue outline shows the Saint-Sorlin Glacier extent in 2015. The three rectangles show the three areas of interest, one outside the glacier and two on the glacier itself with one in the ablation area and the other in the accumulation area.

wet snow in different terrain conditions, as dry snow is nearly transparent at the *C*-band frequency and to separate glacier ice and surrounding rocks ([15], [18], [21], [22], [23] among many other studies). In the case of snow, the radar backscatter depends on the dielectric profiles of the snow and the underlying ground, the roughness of the air–snow and snow–soil boundaries, and the microstructural properties (like grain size, specific surface area, etc.) [24], [25], [26]. At the beginning of the snowmelt, in addition to the decrease in the surface roughness, the dielectric constant of the snowpack increases and the snow layer absorbs most of the radiation emitted by the radar [18], [24], [27]. Snowmelt induces a minimum on SAR signal time series [28], [29].

These properties have led to the extensive use of SAR data to monitor the evolution of the snowpack and glaciers. For instance, Marin et al. [29] have shown that the seasonal variation of SAR backscatters can be used to characterize the three prevailing phases of a melting snowpack. Winsvold et al. [28] used SAR data to map the glacier facies like the superimposed ice area, firn, ice, and wet snow zones. In contrast, Kaushik et al. [30] computed the coefficient of variations of the backscattering signal to analyze ice aprons. Heilig et al. [31] also used the coefficient of variations over glacierized areas to select summer reference images for mapping wet snow. Rott et al. [27] demonstrated that the transient snow line can be tracked with SAR imagery using summer reference images. Scher et al. [32] used a statistical score (z-score) on a time series of backscattering coefficients to estimate melting and frozen periods duration over glaciers. Among all these studies, very few have been dedicated to the analysis of the snow cover in glacierized environments [18]. For this reason, we study the spatio-temporal changes in the snow-covered areas in the catchment of a temperate glacier, with SAR data in *C*-bands from Sentinel-1.

Our first objective is therefore to complement the current state-of-the-art by an in-depth understanding of the variability of the SAR signal in the glacierized environments. We achieve this through a detailed study of the SAR signal near a glacier and in glacier accumulation and ablation zones, in combination with a variety of ancillary data from optical sensors, snowpack models, and expert assessments. Second, we aim to characterize the snowmelt dynamics over different types of surfaces, in an attempt to consolidate and refine wet snow detection methods from SAR observations. We, therefore, exploit methods from the literature and assess their performance with respect to the available data at our study site. This study focuses on the Saint-Sorlin Glacier in the French Alps as a representative example of temperate alpine glaciers.

II. Data and Study Area

A. Location of the Study Area

Saint-Sorlin Glacier is located in the Grandes-Rousses massif of the French Alps [see Fig. 1(b)] and is classified as a temperate glacier. Saint-Sorlin Glacier has been selected as test zone due to the large amount of available meteorological and glaciological data, thanks to the monitoring of the Service National d'Observation Glacioclim. Its altitude ranges from 3400 to 2700 m above sea level (m a.s.l.). At the end of each hydrological year, the glacier can be divided into two areas based on the equilibrium line: the accumulation area, where the snowpack persists at the end of the summer period due to a positive annual surface mass balance, and the ablation area, where the winter snowpack and part of the ice are lost during summer.

Three areas have been selected to track ice/snow evolution as part of the monitoring process for the Saint-Sorlin Glacier catchment. These areas have approximately 500 $\pm$ 10 pixels each, equivalent to almost 50 000 m^2. The three areas of interest (AoI) are named *Rock*, *Abl*, and *Acc*. While the first area is located outside the glacier, the second and third areas are in the glacier's ablation and accumulation areas, respectively. Fig. 1(c) visually represents the three AoIs. Each area has a different altitude: *Rock*, *Abl*, and *Acc* are at 2600–2700, 2800, and 3000 m a.s.l., respectively. The *Rock* AoI is a crucial reference zone for SAR signal characterization.

The three AoIs were carefully selected to avoid any shadow/layover phenomena that might occur due to the use of SAR observations, especially here, because of the series of ridges bordering the glacier. Additionally, other criteria were

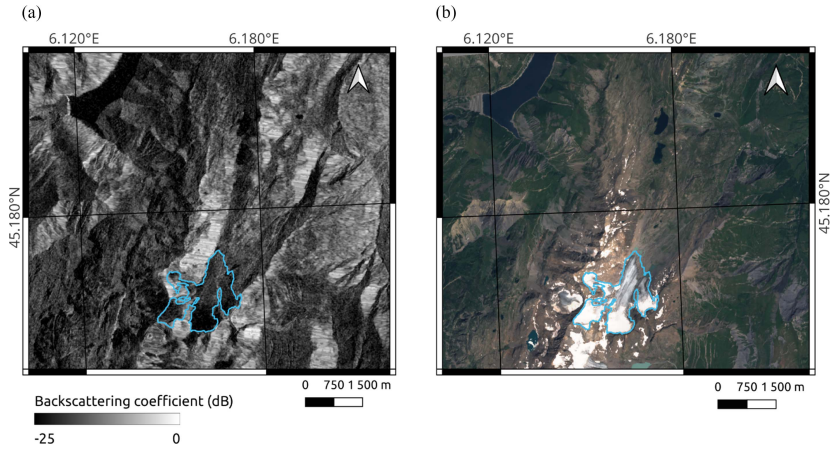

Fig. 2. Satellite images in the vicinity of the Saint-Sorlin Glacier. The light blue outline shows the Saint-Sorlin Glacier extent in 2015. (a) Backscattering coefficient on 5th July 2022, from Sentinel-1 SAR VH-polarized image, in descending orbit. (b) True color image from Sentinel-2 data on 8th July 2022.

taken into consideration while choosing these areas, such as avoiding any presence of water bodies like lakes, streams, or wetlands in the *Rock* area, and ensuring that *Abl* remains completely covered with bare ice at the end of each hydrological year. Similarly, *Acc* was chosen to be located in the firn or snow area during summer, and all three areas were selected as homogeneous as possible to enable effective temporal monitoring.

B. Remote Sensing Data and Validation Data

We used *C*-band SAR intensity images from Sentinel-1 satellites, hereafter referred to as the backscattering coefficient σ_0 (in dB). The Sentinel-1 constellation comprises two satellites, A and B, until the end of 2021, making it possible to observe the Saint-Sorlin Glacier every 6 days, assuming one orbit track. We used both ascending and descending orbits, specifically, the descending relative orbit 139 (passing at 5h45 UTC on day D) and the ascending relative orbit 161 (passing at 17h30 UTC on day D+1). SAR images are preprocessed by the S1 Tiling tool developed by the French National Centre for Space Studies (CNES).[1] During the preprocessing, SAR images are orthorectified to Sentinel-2's Military Grid Reference System (MGRS), based on the Universal Transverse Mercator (UTM) projection. The tile containing Saint-Sorlin Glacier is 31TGL. The time period of the study covers the hydrological years from 2017–2018 to 2020–2021. We preprocessed the SAR data using the CNES PEPS facility[2] to obtain a stack of 20 m resolution colocated SAR images at VV and VH polarizations. In this study, we focus only on VH polarization data.

To evaluate and understand the SAR data, reflectances and snow products from Sentinel-2 data were also used. Only scenes without clouds were selected. These data are easily accessible from the Theia database[3] providing a fractional snow cover (FSC) product very similar to the Sentinel-2-based Copernicus Snow Product [16]. The FSC product was utilized to compute the snow disappearance window (SDW), from which we define as the time period between the date when the first pixel of no-snow appears on a given area and the day when the entire area is snow-free. The FSC product was only used on the area outside the glacier, as it does not distinguish between ice and snow pixels. Additionally, we consider that an uncertainty of +/- 5 days affects this SDW due to Sentinel-2 revisiting cycle. RGB composites were generated by combining bands 11, 8, and 2 from the spectral range of Sentinel-2; they show ice pixels in blue and snow/firn in cyan over the accumulation area [see Fig. 9] [17]. In addition, 23 optical images were obtained from SPOT6/7 sensors from the Kalideos-Alpes project[4] between 2017 and 2019 in order to complete the time series of Sentinel-2 when no images were available. An overview of the Sentinel-1 and Sentinel-2 images above the Saint-Sorlin Glacier is available in Fig. 2.

Data from the Bulletin d'Estimation du Risque d'Avalanches (BERA) were also used. They consist of expert data assembled in forecast bulletins issued daily by the Météo-France weather and risk avalanche forecasters, at the scale of French Alps massifs. They are freely accessible.[5] We specifically used the BERA information on the altitude of the limit between rain and snow, the elevation of the 0 °C isotherm, and the snow height, focusing on the Grandes-Rousses massif where the Saint-Sorlin Glacier is located.

C. The Crocus Snowpack Simulations

To guide our understanding of the SAR signal with respect to the different phases of the snowmelt, we use snowpack simulations carried out with the Crocus snowpack model [33] at the three AoIs. Crocus is a state-of-the-art, detailed, and physics-based snow model widely used to simulate the evolution of alpine snowpacks. It can handle up to 50 snow layers, and represents the snowpack energy and mass balances and its exchanges with the atmosphere and underlying soil. For this application on the three AoIs on or nearby the Saint-Sorlin Glacier in the Grandes-Rousses massif, we use as meteorological forcing the SAFRAN reanalysis [34], [35] that consists

[1][Online]. Available: https://www.github.com/CNES/S1Tiling
[2][Online]. Available: peps.cnes.fr
[3][Online]. Available: theia.cnes.fr
[4][Online]. Available: alpes.kalideos.fr
[5][Online]. Available: https://donneespubliques.meteofrance.fr/?fond=produit&id_produit=265&id_rubrique=50

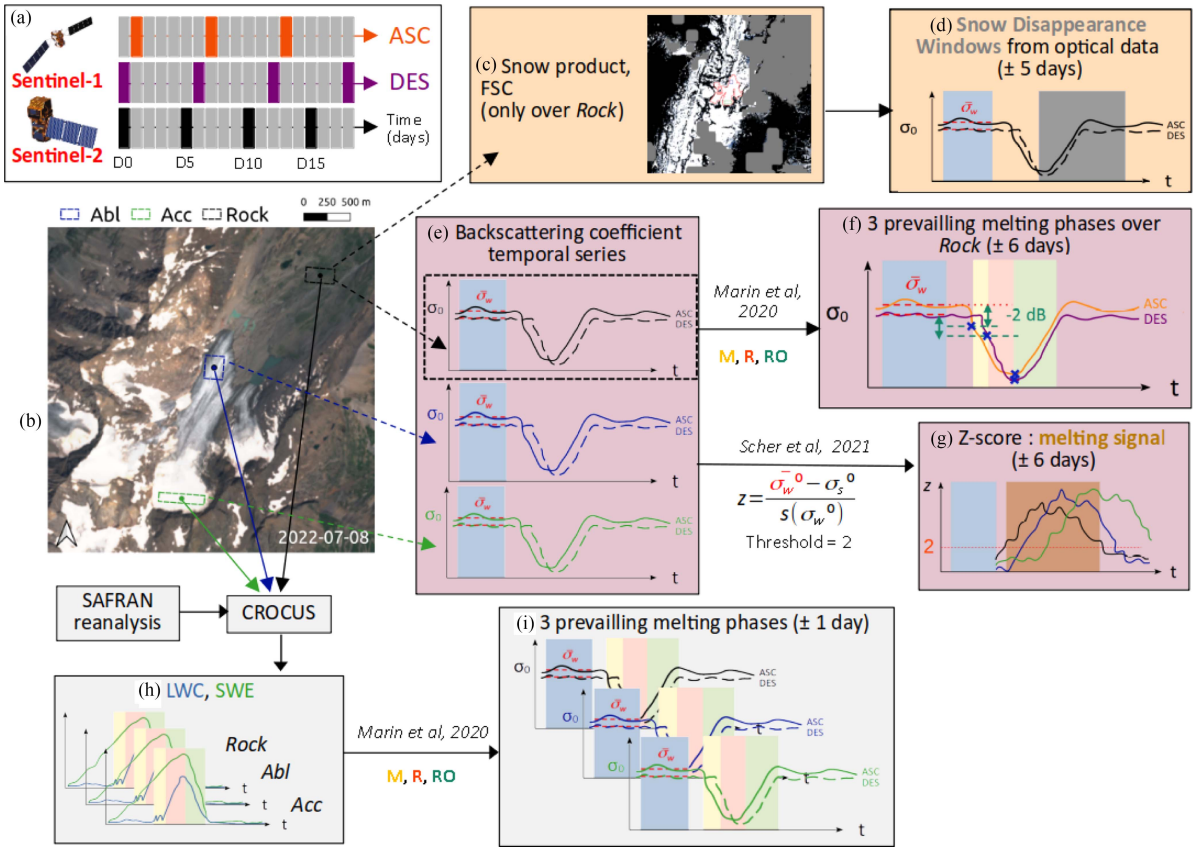

Fig. 3. Summary of our methodological approach. (a) Passing frequency for Sentinel-1 (both orbits: ascending and descending) and Sentinel-2. (b) True color image from Sentinel-2 data (8 July 2022) over Saint-Sorlin Glacier, with the three study areas and their centroïds. (c) FSC from snow product Copernicus. (d) SDWs over *Rock*. (e) Backscattering coefficient temporal series from Sentinel-1. (f) Marin et al. [29] method used directly on SAR data to get melting phases over *Rock*, adapted from Marin et al. [29]. Melting phases are represented in yellow for M phase, red for R phase, and green for RO phase. (g) Computing the z-score on each AoI. (h) LWC and SWE simulations from Crocus snowpack model. (i) Melting phases extracted from Crocus simulations. Each box background color represents a type of data: Purple for SAR images, orange for optical data, and gray for models. The number of days in brackets refers to the related uncertainties.

in global numerical weather forecasts from the ARPEGE numerical weather prediction model, which are fine-tuned with all available mountain meteorological observations. This reanalysis is available at 300 m elevation steps over the French mountain massifs (shown in dark blue outlines on Fig. 1) which are considered climatically homogeneous except for altitude, slope, and orientation effects. This reanalysis is routinely used to estimate the snowpack conditions over the French mountain massifs [35]. The snowpack model Crocus forced by the SAFRAN reanalysis has been largely evaluated against observations of various kinds, pointing toward good performances over the French mountain massifs [35], [36], [37], [38]. In addition, Crocus was part of the most recent intercomparison between snowpack models (ESM-SnowMIP; [39], [40]) and exhibited good scores at a variety of snow sites around the Northern Hemisphere.

For each of the AoI (*Rock*, *Abl*, and *Acc*) the location of the centroid is computed [Table IV, in appendixes], in appendixes), and Crocus simulations are carried out considering the local altitude, orientation, and slope. We use the SAFRAN-Crocus chain in "point simulation" mode, whereby a linear interpolation is applied to the SAFRAN reanalyzes [37], [41]. For the radiation terms, a projection according to slope and orientation is performed [42]. We focus on two critical variables from these simulations: liquid water content (LWC) and snow water equivalent (SWE) using Crocus outputs from October 2017 to October 2021. It is worth noting that these simulations only provide information on seasonal snow (i.e., the firn layer in the accumulation area and the ice surface in the ablation area are not considered in the simulations).

III. Methods

A. Assess the Snowmelt Dynamics From Backscatter Time Series

The phases of snowmelt begin with the moistening (M) of the snowpack surface, which does not affect the SWE but causes LWC values to oscillate between 0 and 1 kg/m^2 due to daily cycles [refer to Fig. 3(h), in yellow] [29], [43]. The melting process is initially detected by the ascending orbit (afternoon) and only later by the descending orbit due to freeze/thaw cycles in the first few days of melting. With increasing temperatures in the course of spring, the snowpack surface does not systematically refreeze at night, leading to an increase in liquid water content and a consequent variation in the backscattering signal seen in SAR imagery. It is important to note that only the ascending

orbit captures the M phase, with a decrease in σ_0 greater than 2 dB [29] [see Fig. 3(f), in yellow].

The second phase of snowmelt is the saturation and ripening phase (R), which occurs when the melting front reaches the base of the snowpack [43]. This phase is characterized by decreasing backscattering signals in the descending orbit [see Fig. 3(f), in red]. The SWE has not started decreasing yet at the end of the R phase, and both the ascending and descending orbits show minimum values [see Fig. 3(h), in red].

The last phase is the run-off (RO) phase, which is triggered when the snowpack progressively loses its liquid water content. Both LWC and SWE decrease until they reach zero kg/m^2 [see Fig. 3(h), in green]. At this point, the snow cover becomes increasingly sparse and heterogeneous, causing the snow depth on the ground from FSC products to overlap with the RO phase. During the RO phase, both ascending and descending SAR signals increase.

We applied the Marin et al. [29] method on the backscatter time series for both orbits to retrieve the three melting phases. For the beginning of the M phase, we used the means of σ_0 over winter periods (referred to as σ_w^0) as the reference values and assumed that our winter period is from 1st January to 1st March. We then applied the mean of the winter preceding the given melt season. We relied on a threshold of -2 dB between σ_0 of spring/summer and the reference values to retrieve moistening and ripening phases. We denote TM, TR, and TRO as the duration of the moistening, ripening, and run-off SAR-based phases, respectively.

We also tested another metric to compute the reference value. For each pixel in an AoI, we computed the 75% quantile for each year over January–February and then took the average over the AoI. We noted the value for a given year i as Q_3^i.

Following Veyssière et al. [36], who found good agreement between Crocus simulations and Sentinel-1 data, we suggest using LWC and SWE to guide us in the determination of the melting phases and assess their estimation with SAR data on the Saint-Sorlin Glacier. In the following analysis, we will compare to the modeling the SAR results considering two reference values, Q3 and winter means, by considering the melting phases modeled with Crocus as a reference. However, Crocus snowpack model tends to underestimate snow accumulation at very high altitudes [44]: it is therefore, more reliable at the melt begining than at the end and Crocus can be used as reference only for the M phases. In the same way as with SAR images, we denote TM*, TR*, and TRO* as the duration of the melting phases retrieved from Crocus simulations, and we use the same thresholds as Marin et al. [29] on LWC and SWE time series. On the *Rock* AoI, we calculate the time lag between the onset of melting phases estimated from Crocus simulations and those obtained from the SAR signal using both reference values. A positive delay indicates an advanced melt event from Crocus compared to the one extracted from Sentinel-1 data. The reference value that provides the lowermost delay is chosen.

B. Characterize Melting Signals With Z-Score

As melting periods are associated with minimum values of backscattering coefficient, they can be characterized by a threshold on σ_0 (i.e., -2 dB with respect to winter means or Q3). Statistical metrics are an appropriate method to characterize the decreasing and increasing of σ_0 and give a temporal indication of these periods: for this reason, Sher et al. [32] used the z-score to evaluate the duration of melt, between the melt onset and the run-off ending. As we are interested in melting events, we computed the z-score over a year without winter periods and we used the same winter period as defined above. For a given hydrological year, the z-score is defined as follows [32]:

$$z = \frac{\overline{\sigma_w^0} - \sigma_s^0}{s(\sigma_w^0)} \tag{1}$$

with $\overline{\sigma_w^0}$ the winter mean computed on January–February, $s(\sigma_w^0)$ the standard deviation over the same winter period, and σ_s^0 the backscattering coefficient in summer (i.e., out of winter periods).

There are differences between the methods used by Marin et al. [29] and Scher et al. [32] to determine the melting signal occurrences. Marin et al. method indicates with precision the three main melting phases, while Scher et al. [32] gives a coarser information on the melting periods. Scher et al. [32] compute the z-score for each pixel of a given area on both orbits and keeps only the orbit that maximizes the score. Then, a threshold of 2 (no unit) is applied to the temporal series of z-score to determine the melting signal occurrences. The temporal uncertainty on the z-score is 6 days due to the repeat time of Sentinel-1.

Fig. 3 shows a schematic representation of the data and methods used in this study.

IV. Results

A. Comparison of SAR and Optical Data Over Rock AoI.

We first characterize the evolution of the SAR signal over the *Rock* AoI located on the glacier foreland. The SDW determined for each year from the FSC products is shown in dark-gray in Fig. 4(a). As Sentinel-2 cannot make the difference between wet and dry snow, we can only see when the snow cover fraction declines, which happens during the run-off phase. Therefore, the run-off phase as defined by Marin et al. [29] and the SDW extracted from FSC products must appear at the same time.

For the years 2017 and 2019, the length of the SDW is significantly shorted, i.e., 60 and 50 days, respectively, compared to the other years for which the SDW ranges between 85 and 115 days. For the year 2019, the short SDW can be related to the limited snow accumulation of the 2018–2019 winter (maximum snow thickness of 2.6 m at 2500 m a.s.l., according to BERA data, compared to an average of 3.2 m over the period 2016–2022), leading to a thinner snowpack that melted faster. On the other hand, winter 2018 has the longest SDW and it can be linked to the wettest winter of the decades, with accumulation amounts reaching 4.7 m at 2500 m a.s.l. according to the BERA data.

It should be noted that the SDW may have a significant degree of uncertainty. This is due to the presence of clouds at high altitudes and the limited availability of cloud-free images, which are acquired only every 5 days. As a result, accurately identifying the limit of the melting period may not be optimal. This was particularly the case in spring 2017, when cloud-free Sentinel-2 images are very few. For instance, in the image acquired on May 10th, the ground is fully covered with snow (according to FSC product). The following usable image was acquired on June 19th; but on this image the *Rock* AoI was already snow-free for

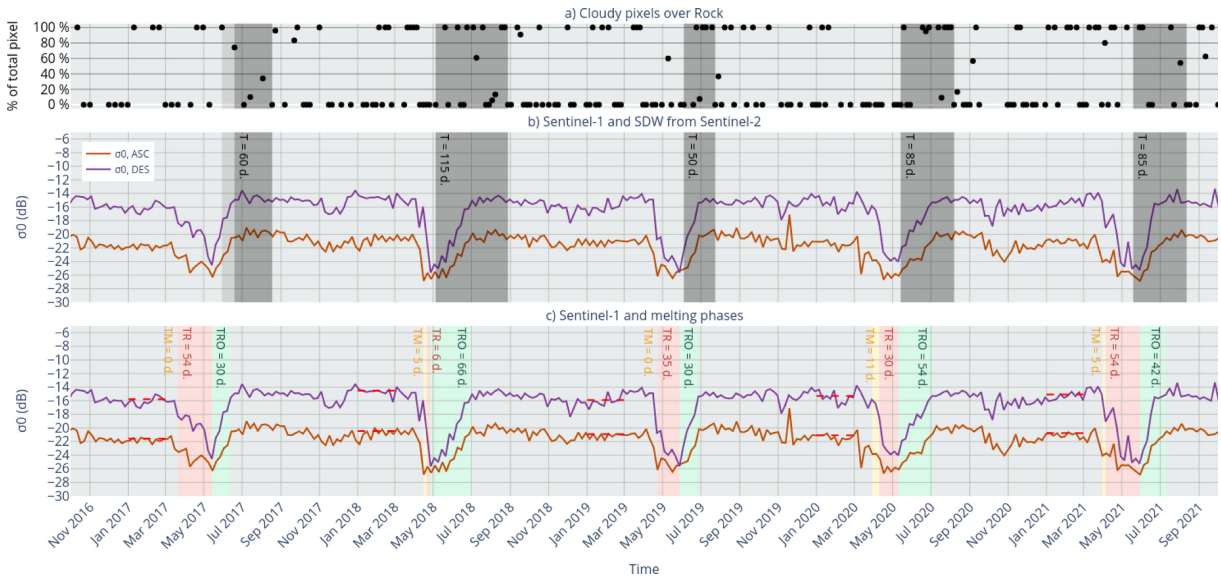

Fig. 4. Time series of backscattering coefficient over the *Rock* AoI. Both orbits are shown (ASC for ascending and DES for descending orbit). (a) The percentage of cloudy pixels retrieved from Sentinel-2 images is represented with black dots (extracted from the FSC product). (b) SDWs quantified from the optical images Sentinel-2 are shown in dark-gray, with their duration T expressed in days. For 2017 only, uncertainties on the SDW beginning is plotted in lighter gray. (c) For each hydrological years, three snowmelt phases are discerned using the method developed by Marin et al. [29] with the Q3 threshold. Threshold computed from Q3 are also plotted in red dashed lines.

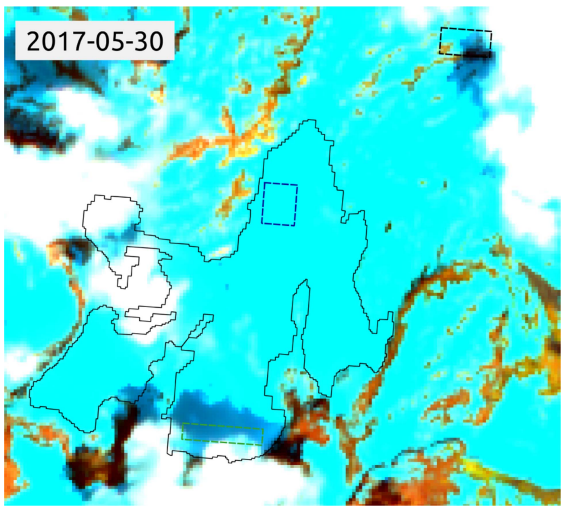

Fig. 5. RGB composites from Sentinel-2 images (bands 11, 8, and 2) over Saint-Sorlin Glacier, on the 30 May 2017. Outlines of the AoI are shown.

26% of the pixels, and the cloud cover was important on the image (the remaining 74%). Therefore, the disappearance of the snow cover over the *Rock* AoI has started well before June 19th, which gives considerable uncertainty about the beginning of the SDW. Indeed, even if FSC product indicates a zone entirely under clouds on May 30th, *Rock* has several snow-free pixels on the optical image at the same date [see Fig. 5]. It is why we decided to put a lighter gray in the time range between May 30th and June 19th in Fig. 4(a). May 2021 was another example of numerous Sentinel-2 images with an important cloud cover.

In Fig. 4(a), we compare the SAR signal over the *Rock* AoI with the SDW. A good agreement is seen between SAR and optical data: the increase in the SAR signal appears during the snowmelt windows (except for 2017 for the reasons stated above).

We use the descending orbit for comparing the SAR signal minimum and the beginning of the SDW. Only the descending orbit provides information on snow cover disappearance, as it sees freeze/thaw cycles in the morning, and therefore the melting events after the ascending orbit. The backscatter coefficients reach their minimum well before the SDW starts. In 2018, pixels started becoming snow-free 8 days after the σ_0 minimum, while in 2019, it was 7 days, and in 2020 only 4 days (+/- 5 days). The 2021 season was exceptional as Sentinel-2 detected snow-free pixels over *Rock* 10 days (+/- 5 days) before the σ_0 minimum.

In most cases, the snow loss continues even if the SAR signal is stable for both orbits. Depending on the year, this process can take 1 to 2 months after stabilization. For instance, there was a 66-day difference in 2017, 57 days in 2018, 27 days in 2019, 35 days in 2020, and 33 days in 2021. Once again, the cloud coverage and the 5-d frequency of Sentinel-2 image acquisition may explain why the SDW lags after the backscatter minimum.

B. Comparison of SAR Data and Crocus Simulations on Rock *AoI*

Fig. 6 shows the temporal evolution of the LWC and SWE simulated by Crocus for the *Rock* AoI. To extract the modeling-based melting phases, we followed the methodology proposed in Marin et al. [29]. The winters of 2016–2017 and 2017–2018 show strong differences, with the former being the driest and the latter being the wettest.

We thus compute the three phases with the SAR signal using the winter-averaged [see appendixes, Fig. 11] and the Q3

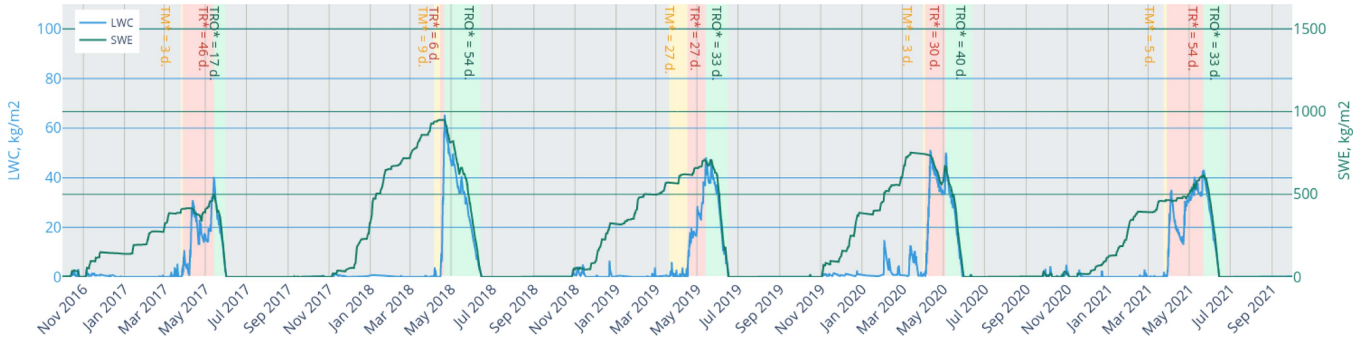

Fig. 6. Time series of LWC and SWE, from Crocus simulations over *Rock* centroïd point. Colored stripes represent the melting phases retrieved using LWC and SWE, as defined by Marin et al. [29]: Moistening phase in yellow, ripening phase in red, and run-off in green. Duration of each phase is written (TM, TR, and TRO).

TABLE I
REFERENCE VALUES FOR BOTH METHODS Q3 AND WINTER-MEANS, BY ORBIT AND BY YEARS (IN dB)

Winter-mean	2017	2018	2019	2020	2021
ASC	−22.1	−21.3	−21.6	−21.7	−21.5
DES	−16.8	−15.6	−16.6	−16.436	−16.3
Q3	2017	2018	2019	2020	2021
ASC	−21.6	−20.5	−20.9	−21.1	−20.8
DES	−15.8	−14.5	−15.9	−15.3	−15.1

TABLE II
TIME DIFFERENCE (IN DAYS) BETWEEN THE START OF MELTING PHASES EXTRACTED FROM CROCUS SIMULATIONS AND THOSE EXTRACTED FROM SENTINEL-1 DATA

a) With winter means as reference value

Melt phases	2017	2018	2019	2020	2021	Mean
M	14	1	32	−2	3	**9.6**
R	16	6	5	6	7	**8**
RO	0	6	14	6	7	**6.6**

b) With Q3 as reference value

Melt phases	2017	2018	2019	2020	2021	Mean
M	−5	1	32	−2	3	**5.8**
R	−8	6	5	6	7	**3.2**
RO	0	6	14	6	7	**6.6**

Bold value indicate the averages of time differences for each melting phase.

reference values [see Fig. 4(b)] and also taking into account the two orbits. Whatever the year, Q3 values are greater than winter-averaged ones [see Table I]. The temporal differences between the beginning of the first melting phase quantified from Crocus and from the SAR signal, are lower considering Q3 as the reference values [see Table II; the Q3 reference values are shown in red dashed line in Fig. 4(b)]. This leads us to consider Q3 as a more suitable reference value for the determination of the melt onset.

Fig. 4(a) and (b) shows that for each year, the SDW overlaps the run-off phase with a time difference of a few days in agreement with the 5-d acquisitions of Sentinel-2, except for the year 2017 because of the reasons exposed previously related to cloud cover.

C. *Cross-Analysis With Z-Score Over* Rock, Abl, *and* Acc *AoI*

Fig. 7 shows the temporal evolution of the backscattering coefficient over *Abl* and *Acc* AoI. At first glance, the SAR signal is completely different from that of *Rock*. Indeed, both orbits show a close evolution of the backscattering values on the *Abl* AoI. For the *Acc* AoI, σ_0 values show a greater difference between the two orbits for the maximal σ values. We also notice that, on average, σ_0 values from the ascending orbit are higher than the descending one over *Acc* and *Abl*, which is the contrary over the *Rock* AoI. The differences in the SAR signals between the ascending and descending orbits are due to a difference in the angle of incidence. The period of minimum backscattering values, where SAR signal is under its winter means minus 2 dB, lasts longer for *Abl* and *Acc* (around 7 months) compared to *Rock* (between 2 and 3 months). For *Abl*, backscattering coefficient is below the threshold of wet snow (defined as Q3 −2 dB, according to our precedent results) for about 236 and 204 days for ascending and descending orbits, respectively. The accumulation area is characterized by 210 and 208 days when σ_0 is below this threshold, for ascending and descending orbits, respectively.

In winter, the accumulation area shows a larger amplitude difference between ascending and descending orbits with respect to the ablation area. *Acc* AoI has the smallest mean of Q3 reference values: Q3 mean over the five studied years of −12.12 and −15.94 dB for ascending and descending orbits, respectively. The *Abl* AoI Q3 reference value is comprised between the ones of *Rock* and *Acc* AoI: with a mean of −16.51 and −17.69 dB for ascending and descending orbits, respectively. It agrees well with Winsvold et al. [28] who found that σ_0 increases with altitude, whatever the period of year.

We note that the σ_0 decrease is sharper for the two AoI over the glacier around mi April and May. On the contrary, the increase in backscattering occurs slowly. For both orbits, two stages stand out for *Abl* AoI on Fig. 7, which are linked to two different states of the surface: snow-covered surface and bare ice surface. After the strong decrease from the first stage, σ_0 is stabilized around its minimum values: the snowpack from the previous winter precipitations is melting. Then, σ_0 increases to an intermediate stage between the first one and its minimum value. It is the transition from a snow-covered surface to a bare ice surface: the total snow depth of the previous winter has melted and the ice surface has begun to melt (see the transient snow line evolution on Fig. 2 from Winsvold et al. [28]). Finally, the SAR signal reaches values of the first stage; the melt season is over and a new winter season starts with the establishment of the snowpack. It is clear that the Marin et al. method cannot be directly applied

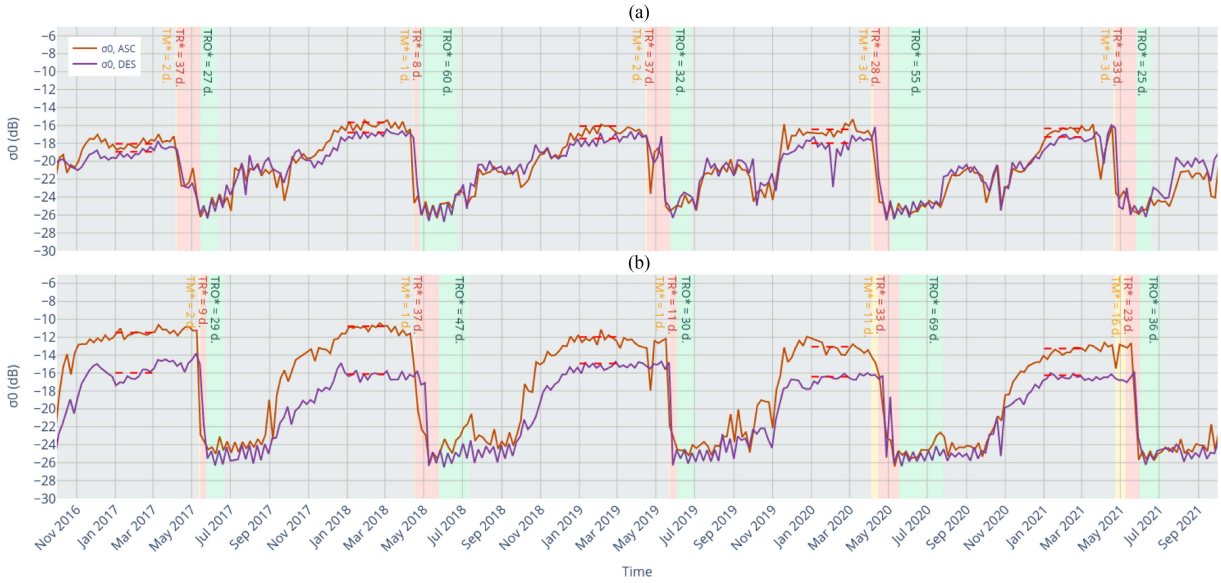

Fig. 7. Time series of backscattering coefficient over (a) *Abl* and (b) *Acc* AoI. Both orbits are shown (ASC for ascending and DES for descending). For each hydrological year, three snowmelt phases are discerned using Crocus simulations. Threshold computed from Q3 are also plotted in red dashed lines, for each area, each winter period and each orbit.

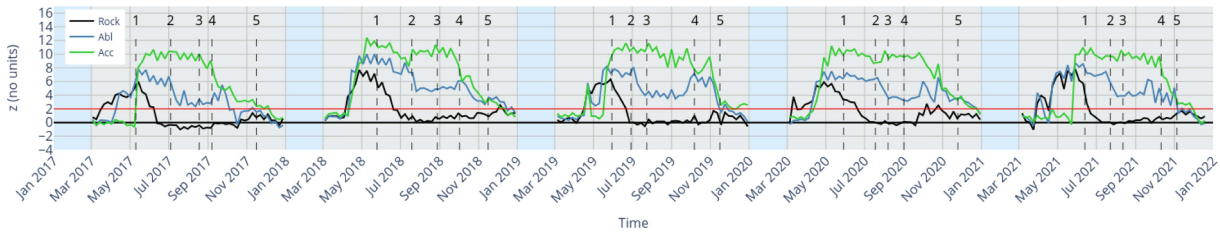

Fig. 8. Time series of z-score over the three AoIs. The red line is the threshold used in Scher et al. [32] method to determine melting periods. Blue rectangles show the winter periods. Numbers (1–5) allow illustrating five main events above Saint-Sorlin Glacier (see details in Section IV-C, and Fig. 9 for the corresponding satellite images).

to SAR time series for *Acc* and *Abl* as the glacier environment is complex and the snowpack does not melt during about 7 months.

Fig. 8 shows the evolution of the z-score computed for the three AoIs. This score allows to characterize the entire duration of the melting season, from the moistening to the end of the run-off phase. First, we analysis the comparison of the two methods for the *Rock* AoI. We expect that the melting periods inferred from z-score will overlap with the three melting phases. By comparing Figs. 4(b) and 8, we see a very good agreement between the start of melting signal in the z-score and the beginning of the moistening phase, except for 2018, with a delay of one week for the M phase. However, the end of the melting signal occurs before the end of the RO phase, with an apparent time lag of about 10 days. In this analysis, year 2021 is standing out with a melting signal 23 days in advance on the M phase beginning, and a 24 days delay on the end of the RO phase.

Plotting the seasonal evolution of the z-score across the different AoIs allows for insightful parallels with optical images [see Figs. 8 and 9]. In the following, we choose five characteristic events, numbered from 1 to 5, for which we identified for each year mostly cloud-free Sentinel-2 scenes when possible (in this case, RGB images of the scenes are shown in Fig. 9).

1) The three AoIs are entirely covered with snow.
2) *Rock* area is snow-free, but snow cover maintains over *Acc* and *Abl*.
3) *Rock* area is still snow-free, the snowline retreat over *Abl*, which surface is totally in bare ice, and *Acc* is covered by snow and firn.
4) The first snowfall of the automn/winter occurs and the three AoIs are snow-covered. But this first snowfall melts quickly and snow-free pixel appears.
5) The snowpack is settling for the following winter season, the three AoIs are fully covered with dry snow.

Melting signals on the glacier AoI are very different from the one of the *Rock* AoI: z-score becomes higher than 2 lately and then hardly goes below 2. This pattern is the same whatever the year. From March to April, z-score increases sharply over all three AoIs and becomes greater than 2 with a delay with the altitude. For *Abl*, the same stages than with σ_0 time series can be described [see Fig. 7(a)]. First, z-score increases sharply from 0 to 8 in April; it matches the beginning of melt and the surface of the glacier ablation area is still under snow [event n°1, Fig. 9(a), (f), (k), (p), and (u)]. Then, z-score values oscillate between 6 and 8, and these of σ_0 are around -25 dB. During the first stage, the snowpack above ice layer melts and progressively disappears.

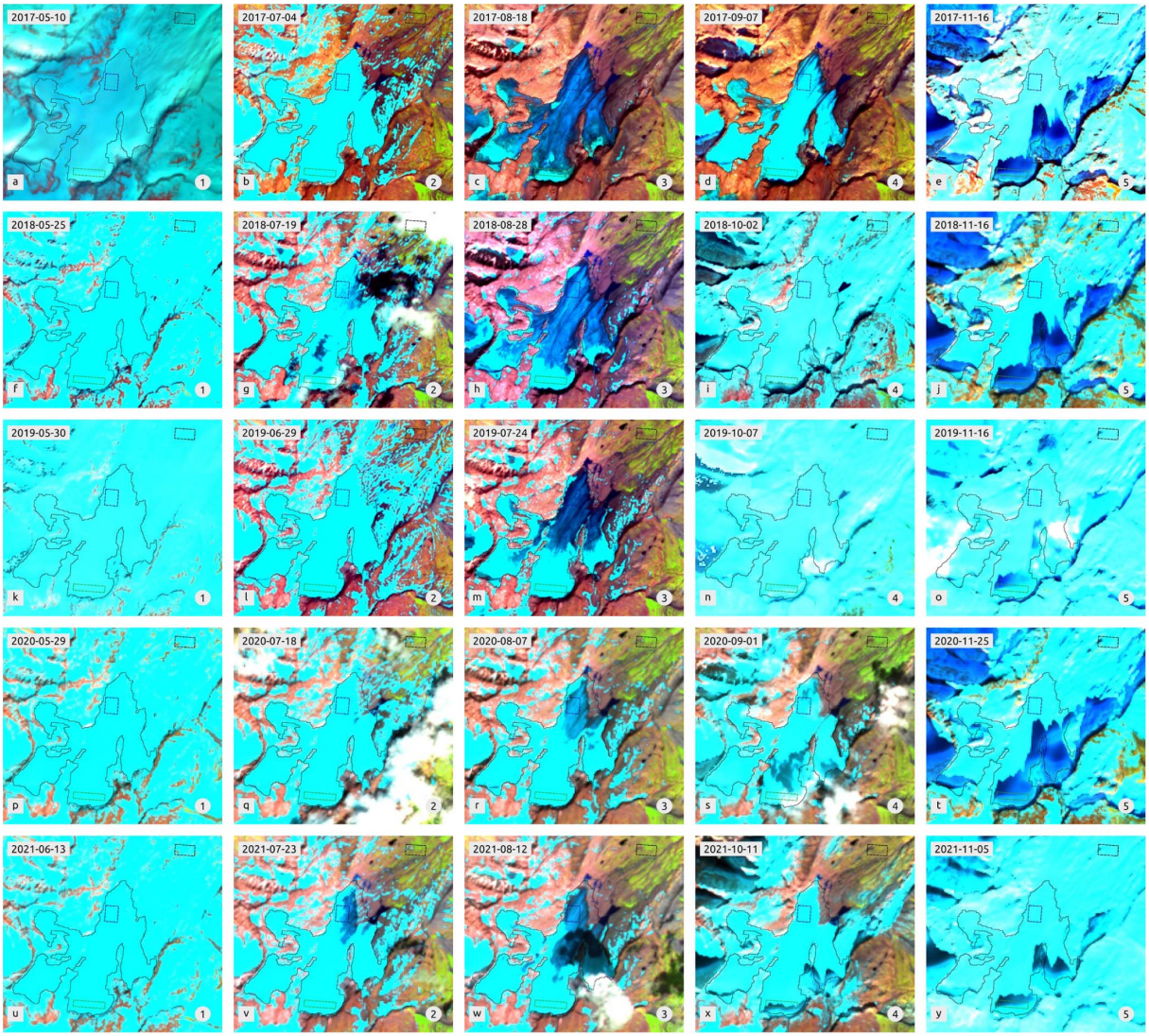

Fig. 9. Set of RGB composites from Sentinel-2 images (bands 11, 8, and 2) over Saint-Sorlin Glacier: in 2017 (a)–(e), 2018 (f)–(j), 2019 (k)–(o), 2020 (p)–(t), and 2021 (u)–(y). For each year, the number (from 1 to 5) written in the low-right corner is directly linked to the events identified on Fig. 8. Ice pixels are seen in blue/dark blue, and snow/firn surfaces appear in cyan.

Abl AoI is still covered by snow for the event n°2 [Fig. 9(b), (g), (l), (q), and (v)], but the snowline goes up over the ablation zone of the glacier and icy pixels within the *Abl* AoI start to appear, until the surface only comprises bare ice, as seen for the event n°3 [Fig. 9(c), (g), (m), (r), and (w)]. With the snow disappearance over this AoI, the z-score decreases to the second stage (around 4) and σ_0 increases to -20 dB. This second stage is linked to the melting of the glacier ice. Between September and November, a brief increase in the z-score value is linked to the first snowfalls during the late summer–early autumn and the shifts between short lasting snowlayers, which rapidly melt. Finally, the z-score decreases below 2 showing that the melt is over and the establishment of the snowpack of the next winter season begins.

The z-score seasonal evolution is more straightforward to analyze for *Acc*. It sharply increases at the beginning of melt season reaching maximum values during the summer months (June–September) and then it slowly decreases around 2 when the next winter season starts. Z-score variations hold only one stage, because surface conditions on accumulation zone remain the same during the melting season (firn). Quite obviously, the z-score values show that melt occurs later at higher altitudes: the melting signal is first seen over *Rock*, then over *Abl*, and finally, *Acc*. Table III shows the gradual withdrawal of the snowline across *Rock* and *Abl*, retrieved with Sentinel-2 optical images [see Fig. 9]. Snowline first retreats itself on *Rock*, and then over *Abl* with a dephasage of about two weeks.

Finally, once the snowpack is settling (in October or November, depending on the year), melting signal disappears on all three AoIs (the z-score becomes smaller than 2) and winter season begins. Snow covers *Acc*, *Abl*, and *Rock* areas, until the next melting season.

Globally, the z-score allows distinguishing the glacier surface state during the melt season. It is particularly visible for the ablation area, where three phases stand out: melting and disappearance of the above snowpack (first stage), then the bare

TABLE III
SNOW COVER DISAPPEARANCE OVER *ROCK* AND *ABL*

Seasons	N	*Rock*	*Abl*
2016–2017	27	04/07	14/07
2017–2018	48	08/08	28/08
2018–2019	48	14/07	24/07
2019–2020	48	23/07	22/08
2020–2021	43	23/07	12/08

Dates for which *Rock* is totally snow-free, and *ABL* surface is on ice; *N* represents the number of FSC images available per seasons over the Saint-Sorlin Glacier (October-September).

ice surface and its melting (second stage), and finally, the first snow fall that rapidly melts at the end of the hydrological year.

D. *Snowpack Simulations Over* Acc *and* Abl *AoI*

To obtain the melting phases on *Acc* and *Abl* AoI, we used Crocus simulations because retrieving them directly from the backscattering coefficient time series was impossible (see Fig. 7). We followed the same procedure as for the *Rock* AoI (refer to Section IV-B for more details). In the appendixes, we plotted the time series of these two variables and the melting phases retrieved from Crocus [see Fig. 12]. The *Acc* area has higher LWC and SWE compared to *Abl* due to a higher elevation and the resulting amount of snow. The maximum values were reached later on *Acc* than on *Abl* because of the altitude difference. We overlaid these melting phases on σ_0 for both orbits in Fig. 7. We observe a strong agreement between the sharp SAR signal drop and the moistening phases beginning. However, unlike *Abl*, the signal of *Acc* did not increase during the run-off phase. Instead, it began to grow only in autumn with the snowfalls of the next winter season, except for 2018 and 2019, where a slight increase in backscattering appears on ascending orbit around mid July for 2018, and at the end of August for 2019. This slight increase is immediately followed by a drop of the same order of magnitude (around 3 dB).

Before the melt season clearly gets underway, there may be very weak melt signals visible on the SAR signal; for example a dry period in winter with temperatures high enough to initiate surface melting of the snowpack, just before snowfall late in season. It is the case at the end of March/start of April 2021: LWC of *Acc* increases from 29/03, reaches a maximum (15 kg/m^2) on 2nd April, and then decreases to 0 kg/m^2 on 9th April. At the same time, the backscattering coefficient reaches two minimum values: 31st March for ascending and 5th April for descending, with a decrease of more than -2 dB. For a reminder, minimum extrema occur lately for descending orbits, as melting happens first during the day, and then during the night when freeze/thaw cycles stop. Furthermore, the elevation of the 0 °C isotherm is very high during this periods: according to BERA, it is higher than to 2800 m a.s.l. between 29th March and 2nd April, and remains around 2300 m a.s.l. until 5th April.

V. DISCUSSION

SAR data give us essential information on surface conditions in the ablation and accumulation zones. We were able to monitor snowmelt in the vicinity of Saint-Sorlin Glacier, thanks to backscatter time series of Sentinel-1. However, monitoring freeze and thaw events using Sentinel-1 has some limitations. For instance, we cannot capture all events that occur on a daily scale. Additionally, with the loss of the Sentinel-1B satellite at the end of 2021, it is even more challenging to monitor freeze and thaw events. Some M phases last for 0 days in 2017 and 2019 over *Rock* AoI, while Crocus simulations show that they last for 3 and 27 days for 2017 and 2019, respectively. However, the 6-day repeat time appears sufficient to monitor melting phases on glaciers and mountainous areas as they last for at least 10 days. Finally, if we are only interested in wet snow cover, we, therefore, only need to know the start of the M phase and the end of the RO phase, and not the duration of each phase in detail.

In this study, we only use the cross-polarization (VH) but as Sentinel-1 is a dual polarization system, it also provides SAR images in copolarization (VV). SAR signals at the *C*-band behave differently with wet and dry snow. It is interesting to note that when snow is dry, SAR signals can penetrate up to a depth of 20 m [45]. However, when the snow melts, the dielectric properties of the snowpack change and the penetration depth decreases to around 3 cm [45]. When the snowpack is dry, the dominant scattering process occurs due to the snowpack volume scattering and the surface scattering at the snow/ground interface. In the case of wet snow, the volume scattering becomes less significant [24]. It is also worth noting that a snowpack is a complex multilayer structure, and its backscattering can be affected by other factors such as snow depth, grain size, and density, among other factors. Observations at *C*-band in cross-polarization may be more sensitive to dry snow accumulation than in copolarization due to weaker surface scattering from the ground and larger volume scattering caused by irregularly shaped and clustered ice crystals in dry snow. As a result, for deep snow often encountered in mountain regions, the scattering from the snow may dominate over the surface scattering from the ground, as noted by Shi and Dozier [46], among others. VV polarization shows greater capabilities to follow the transition toward ice surfaces than VH polarization [47]. For instance, Tom et al. [48] and Stonevicius et al. [49] showed that VV-polarized images are more suitable than VH-polarized one to monitor frozen lake. Kendra et al. [50] found that volume scattering contributions of a dry snow layer were higher with VH-polarized data than copolarized. We evaluated this sensitivity over the ablation area, as it is the only area among our AoI where glacier ice emerges over the course of the summer season [see Fig. 10]. During winter, SAR data with VV polarization over *Abl* have the same evolution as *Rock*, where the backscatter remains almost constant. Then, there are decreases and increases of σ_0 to the same values during winter. Compared with melt phases retrieved with Crocus simulations, we can observe coherence between the minimum extrema of σ_0 and the beginning of run-off. VV polarization appears to be more effective than VH polarization to retrieve the end of snow melt from SAR data over *Abl* AoI. Before the stabilization of the SAR signal, the backscattering coefficient oscillates around winter means, indicating significant variability of surface conditions (plotted in red dashed lines in Fig. 10).

The three AoIs have been carefully chosen but as the front of Saint-Sorlin Glacier retreats further and further [51], the continuation of this study in the future will require to reshape the

Fig. 10. Time series of backscattering coefficient over *Abl*, with VV polarization. Both orbits are shown (ASC for ascending and DES for descending). For each hydrological year, three snow melt phases are discerned using Crocus simulations. Winter-means over January–February months are also plotted in red dashed lines, for each winter period and each orbit.

Abl and *Acc* AoI, according to the position of the equilibrium line and of the glacier front. Working with a centerline along the glacier flow axis is conceivable and allows to overcome this issue. Indeed, Winsvold et al. [28] used it for mapping glaciers facies by altitude slide. Additionally, Saint-Sorlin Glacier is located in a complex topographic domain and a SAR geometric distorsion map would improve the quality of the areas definition, especially to define the *Acc* AoI.

Monitoring melting phases over the accumulation area is more challenging than over the ablation area. It is crucial to assess whether the snow accumulated during winter persists and forms a firn layer, indicating a positive mass balance of the accumulation area or if it has completely melted, resulting in a negative mass balance. The Saint-Sorlin Glacier surface mass balance data from the Glacioclim observatory shows no clear correlation between backscatter variation on the *Acc* AoI and the surface mass balance (not shown). This issue deserves further investigation. An alternative would be to use an appropriate z-score threshold on ice surfaces for detecting melting signals over the *Abl* AoI. For instance, a threshold of 5 would be more appropriate, while on the *Acc* AoI, where the z-score remains constant between May and October, a threshold of 2 would have the same effect.

Finally, we consider here a temperate glacier, but this method could be applicable on different types of glaciers. Among the glacier diversity, we can cite cold glaciers, which are characterized by a superimposed ice area between the ablation and accumulation zone at the end of the summer [52]. On the other hand, tropical glaciers show a glaciological regime and precipitations seasonality different from temperate alpine glaciers [13]. In both cases, specific studies would be deserved to assess the transferability of the method.

VI. Conclusion

SAR-based remote sensing has proven to be an effective tool for monitoring some properties of snow and glaciers. The melting phases of the Saint-Sorlin Glacier have been inferred and analyzed using Sentinel-1 SAR images. The snow melt dynamics observed from Sentinel-1 outside the glacier area has a good correlation with the snow pack disappearance seen by Sentinel-2 during the run-off phase. In addition to backscatter information, the Crocus snowpack model is used to simulate the melting phases from liquid water content and snow water equivalent. The Crocus simulations and satellite observations show a good match, with the snowpack model triggering melt about 5–10 days in advance of the SAR time series. The temporal resolution of Crocus, which can provide simulations at hourly timesteps and even below, allows for greater precision in the duration of melting phases compared to SAR data and its 6-day revisiting. The study uses two reference values, the winter average on January–February, and the 75% quantile during the same period, to determine moistening and ripening phases over the *Rock* area.

The method used to study the area outside the glacier with snowpack simulations has now been extended to the glacier areas. Additionally, z-score analysis was added to characterize SAR signals above the accumulation and ablation areas. By using optical images from Sentinel-2, we were able to highlight the links between the surface conditions and SAR signal variations. Furthermore, Sentinel-1 data provided information on the total melting period of snow, the duration of ice ablation, and the first snowfall over the ablation area. However, for the accumulation area, surface conditions remained on firn/snow, and no information on the end of snow melting was inferred from the SAR signal. To monitor wet snow on glaciers, snowpack simulations and knowledge of ablation and accumulation areas or equilibrium line position are necessary, as SAR signal variations are very different between ablation and accumulation areas. To improve wet snow detection in the ablation area, we propose to explore VV-polarized SAR images. However, for accumulation areas, it is even more challenging to derive useful information about melting from SAR data, and snowpack simulations are required to obtain information on melting periods and wet snow cover.

Another alternative is to explore the use of SAR-based images at *L*- and *X*-bands, such as data from ALOS-2, TerraSAR-X, or PAZ. A comprehensive study on the information content of SAR data, depending on the observation band in different locations of the glacier, would be helpful. In addition, applying similar methods used for the Saint-Sorlin Glacier to other temperate glaciers would help to confirm the results and provide a better understanding of the impact of varying polarization, and varying bands. This would help in identifying the most suitable parameter for detecting melting signals on different parts of the glacier. Further research in this direction would be beneficial in improving our knowledge of the accumulation and ablation patterns of alpine glaciers.

APPENDIX

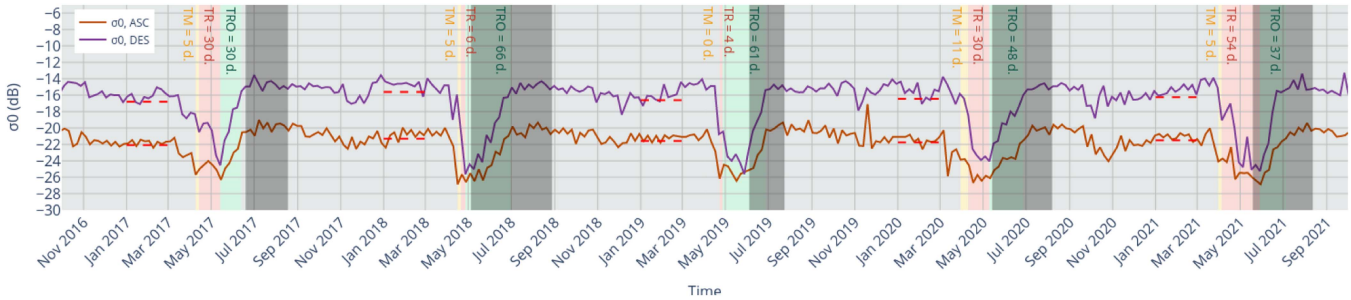

Fig. 11. Same as Fig. 4(b), but using winter mean threshold to retrieve melting phases (see Table I).

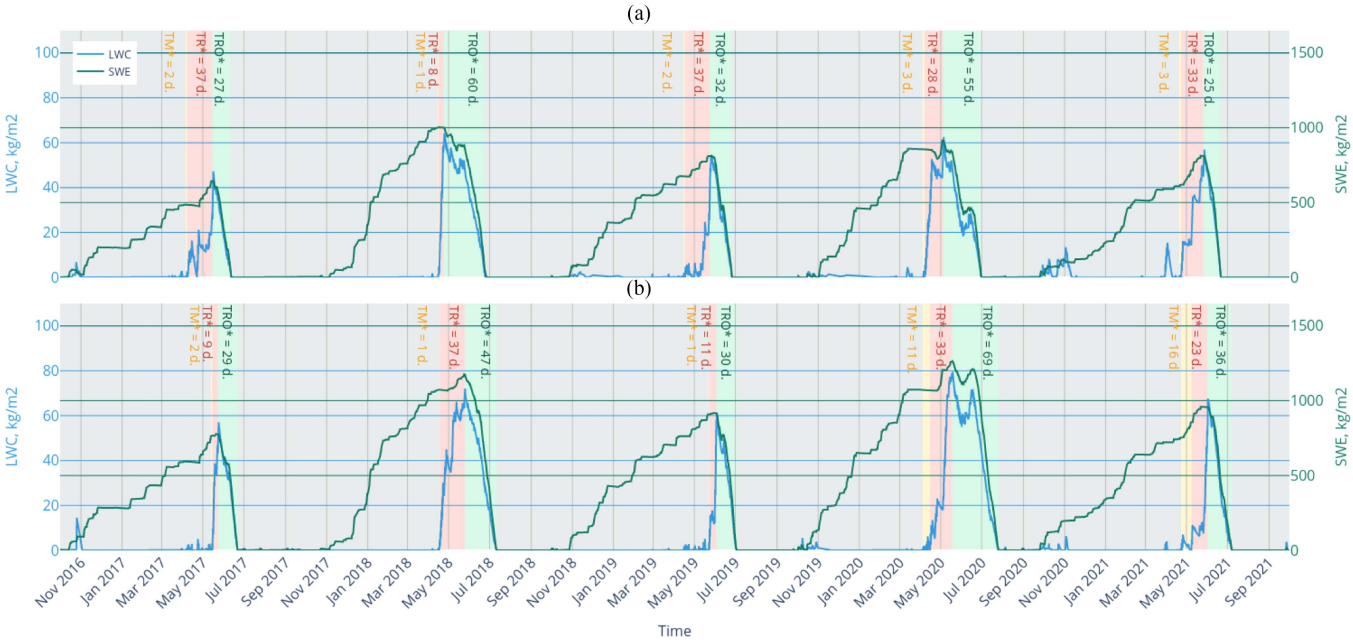

Fig. 12. Same as Fig. 6, but for (a) *Abl* and (b) *Acc* areas.

TABLE IV
COORDINATES OF THE CENTROIDS FROM EACH AOI, EXPRESSED IN THE REFERENCE FRAME RGF93, LAMBERT-93 (EPSG:2154)

Centroïdes	Latitude (Y)	Longitude (X)
Rock	949529	6457879
Abl	948466	6456805
Acc	948223	6455372

ACKNOWLEDGMENT

The authors would like to thank the Service National d'Observation GLACIOCLIM (CNRS-INSU program, OSUG, IRD, INRAE, IPEV, Météo-France) for the data provided. The authors would like to thank A. Racoviteanu and L. Charrier for fruitful discussions. The authors would also like to thank M. Fructus for his help with the Snowtools product to study Crocus simulations. The authors would also like to thank:

1) the support provided by the PNTS French program (Programme National de Télédétection Spatiale);

2) the support provided by the French Space Agency CNES through the project APR SHARE;

3) the support provided by the French Space Agency CNES for preprocessing SAR images with STiling chain;

4) CNRM and IGE are members of Labex OSUG.

The authors would also like to thank the Associate Editor Prof. J. Li and the two anonymous reviewers for comments during the revision process which helped to improve the manuscript.

REFERENCES

[1] D. Vaughan et al., "Observations: Cryosphere," in *Climate Change 2013: The Physical Science Basis. Contribution of Working Group I to the Fifth Assessment Report of the Intergovernmental Panel on Climate Change*, T. Stocker et al., Eds. Cambridge, U.K.: Cambridge Univ. Press, 2013, sec. 4, pp. 317–382.

[2] C. Vincent, "Influence of climate change over the 20th century on four french glacier mass balances," *J. Geophysical Res.: Atmos.*, vol. 107, no. D19, pp. ACL 4–1–ACL 4–12, 2002.

[3] M. Réveillet et al., "Relative performance of empirical and physical models in assessing the seasonal and annual glacier surface mass balance of Saint-Sorlin Glacier (French Alps)," *Cryosphere*, vol. 12, no. 4, pp. 1367–1386, Apr. 2018.

[4] R. Hock et al., "High Mountain Areas," in *IPCC Special Report on the Ocean and Cryosphere in a Changing Climate*, H.-O. Pörtner et al., Eds. Cambridge, U.K.: Cambridge Univ. Press, 2019, pp. 131–202.

[5] C. Vincent, G. Kappenberger, F. Valla, A. Bauder, M. Funk, and E. Le Meur, "Ice ablation as evidence of climate change in the Alps over the 20th century," *J. Geophysical Res.: Atmos.*, vol. 109, no. D10, pp. 1–9, 2004.

[6] D. Six, C. Vincent, M. Bonnefoy-Demongeot, E. Thibert, and P. René, "2022 : Année record pour la fonte des glaciers Français," *La Météorologie*, vol. 2023, no. 120, pp. 13–15, 2023.

[7] J. Faillettaz, M. Funk, and C. Vincent, "Avalanching glacier instabilities: Review on processes and early warning perspectives," *Rev. Geophys.*, vol. 53, no. 2, pp. 203–224, 2015.

[8] M. Beniston et al., "The European mountain cryosphere: A review of its current state, trends, and future challenges," *Cryosphere*, vol. 12, no. 2, pp. 759–794, Mar. 2018.

[9] D. Six and C. Vincent, "Sensitivity of mass balance and equilibrium-line altitude to climate change in the french alps," *J. Glaciol.*, vol. 60, no. 223, pp. 867–878, Jan. 2014.

[10] W. S. B. Paterson, *The Physics of Glaciers*, 3rd ed. Oxford, U.K.: Elsevier, 1994.

[11] A. Rabatel, J.-P. Dedieu, and C. Vincent, "Using remote-sensing data to determine equilibrium-line altitude and mass-balance time series: Validation on three french glaciers 1994–2002," *J. Glaciol.*, vol. 51, no. 175, pp. 539–546, 2005.

[12] A. Rabatel, J. P. Dedieu, and C. Vincent, "Spatio-temporal changes in glacier-wide mass balance quantified by optical remote sensing on 30 glaciers in the french Alps for the period 1983–2014," *J. Glaciol.*, vol. 62, no. 236, pp. 1153–1166, Dec. 2016.

[13] A. Rabatel et al., "Can the snowline be used as an indicator of the equilibrium line and mass balance for glaciers in the outer tropics?," *J. Glaciol.*, vol. 58, no. 212, pp. 1027–1036, Jan. 2012.

[14] R. Marti, S. Gascoin, E. Berthier, M. de Pinel, T. Houet, and D. Laffly, "Mapping snow depth in open alpine terrain from stereo satellite imagery," *Cryosphere*, vol. 10, no. 4, pp. 1361–1380, Jul. 2016.

[15] S. H. Winsvold, A. Kääb, and C. Nuth, "Regional glacier mapping using optical satellite data time series," *IEEE J. Sel. Topics Appl. Earth Observ. Remote Sens.*, vol. 9, no. 8, pp. 3698–3711, Aug. 2016.

[16] S. Gascoin et al., "Estimating fractional snow cover in open terrain from sentinel-2 using the normalized difference snow index," *Remote Sens.*, vol. 12, no. 18, 2020, Art. no. 2904.

[17] F. Paul, S. H. Winsvold, A. Kääb, T. Nagler, and G. Schwaizer, "Glacier remote sensing using Sentinel-2. Part II: Mapping glacier extents and surface facies, and comparison to landsat 8," *Remote Sens.*, vol. 8, no. 7, p. 575, Jul. 2016.

[18] Y.-L. S. Tsai, A. Dietz, N. Oppelt, and C. Kuenzer, "Remote sensing of snow cover using spaceborne SAR: A review," *Remote Sens.*, vol. 11, no. 12, Jan. 2019, Art. no. 1456.

[19] F. T. Ulaby, P. C. Dubois, and J. van Zyl, "Radar mapping of surface soil moisture," *J. Hydrol.*, vol. 184, no. 1, pp. 57–84, 1996.

[20] R. Bamler, "Principles of synthetic aperture radar," *Surv. Geophys.*, vol. 21, no. 2, pp. 147–157, 2000.

[21] M. König, J.-G. Winther, and E. Isaksson, "Measuring snow and glacier ice properties from satellite," *Rev. Geophys.*, vol. 39, no. 1, pp. 1–27, 2001.

[22] T. Nagler and H. Rott, "Retrieval of wet snow by means of multitemporal SAR data," *IEEE Trans. Geosci. Remote Sens.*, vol. 38, no. 2, pp. 754–765, Mar. 2000.

[23] F. Karbou et al., "Monitoring wet snow over an alpine region using Sentinel-1 observations," *Remote Sens.*, vol. 13, no. 3, Jan. 2021, Art. no. 381.

[24] J. Shi and J. Dozier, "Inferring snow wetness using C-band data from SIR-C's polarimetric synthetic aperture radar," *IEEE Trans. Geosci. Remote Sens.*, vol. 33, no. 4, pp. 905–914, Jul. 1995.

[25] N. Baghdadi, Y. Gauthier, M. Bernier, and J.-P. Fortin, "Potential and limitations of RADARSAT SAR data for wet snow monitoring," *IEEE Trans. Geosci. Remote Sens.*, vol. 38, no. 1, pp. 316–320, Jan. 2000.

[26] D. Floricioiu and H. Rott, "Seasonal and short-term variability of multi-frequency, polarimetric radar backscatter of alpine terrain from SIR-C/X-SAR and AIRSAR data," *IEEE Trans. Geosci. Remote Sens.*, vol. 39, no. 12, pp. 2634–2648, Dec. 2001.

[27] H. Rott, "Synthetic aperture radar capabilities for snow and glacier monitoring," *Adv. Space Res.*, vol. 4, no. 11, pp. 241–246, 1984.

[28] S. H. Winsvold, A. Kääb, C. Nuth, L. M. Andreassen, W. J. J. van Pelt, and T. Schellenberger, "Using SAR satellite data time series for regional glacier mapping," *Cryosphere*, vol. 12, pp. 867–890, 2018.

[29] C. Marin et al., "Use of sentinel-1 radar observations to evaluate snowmelt dynamics in alpine regions," *Cryosphere*, vol. 14, no. 3, pp. 935–956, 2020.

[30] S. Kaushik et al., "Analysis of the temporal evolution of ice aprons in the mont-blanc massif using X and C-band SAR images," *Front. Remote Sens.*, vol. 3, 2022, Art. no. 930021.

[31] A. Heilig, A. Wendleder, A. Schmitt, and C. Mayer, "Discriminating wet snow and firn for alpine glaciers using Sentinel-1 data: A case study at Rofental, Austria," *Geosciences*, vol. 9, no. 2, Feb. 2019, Art. no. 69.

[32] C. Scher, N. C. Steiner, and K. C. McDonald, "Mapping seasonal glacier melt across the Hindu Kush Himalaya with time series synthetic aperture radar (SAR)," *Cryosphere*, vol. 15, no. 9, pp. 4465–4482, Sep. 2021.

[33] V. Vionnet et al., "The detailed snowpack scheme crocus and its implementation in SURFEX v7.2," *Geoscientific Model Develop.*, vol. 5, no. 3, pp. 773–791, 2012.

[34] Y. Durand, E. Brun, L. Merindol, G. Guyomarc'h, B. Lesaffre, and E. Martin, "A meteorological estimation of relevant parameters for snow models," *Ann. Glaciol.*, vol. 18, pp. 65–71, Jan. 1993.

[35] M. Vernay et al., "The S2M meteorological and snow cover reanalysis over the French mountainous areas: Description and evaluation (1958–2021)," *Earth Syst. Sci. Data*, vol. 14, no. 4, pp. 1707–1733, Apr. 2022.

[36] G. Veyssière, F. Karbou, S. Morin, M. Lafaysse, and V. Vionnet, "Evaluation of sub-kilometric numerical simulations of C-band radar backscatter over the French Alps against Sentinel-1 observations," *Remote Sens.*, vol. 11, no. 1, Jan. 2019, Art. no. 8.

[37] J. Revuelto et al., "Multi-criteria evaluation of snowpack simulations in complex alpine terrain using satellite and in situ observations," *Remote Sens.*, vol. 10, no. 8, 2018, Art. no. 1171.

[38] F. Karbou, G. James, M. Fructus, and F. Marti, "On the evaluation of the SAR-based copernicus snow products in the French Alps," *Geosciences*, vol. 12, no. 11, p. 420, 2022, Art. no. 420.

[39] G. Krinner et al., "ESM-SnowMIP: Assessing snow models and quantifying snow-related climate feedbacks," *Geoscientific Model Develop.*, vol. 11, no. 12, pp. 5027–5049, Dec. 2018.

[40] C. B. Ménard et al., "Scientific and Human Errors in a Snow Model Intercomparison," *Bull. Amer. Meteorological Soc.*, vol. 102, no. 1, pp. E61–E79, Jan. 2021.

[41] V. Vionnet, I. Dombrowski-Etchevers, M. Lafaysse, L. Quéno, Y. Seity, and E. Bazile, "Numerical weather forecasts at kilometer scale in the french alps: Evaluation and application for snowpack modeling," *J. Hydrometeorol.*, vol. 17, no. 10, pp. 2591–2614, Oct. 2016.

[42] A. Haddjeri et al., "Exploring the sensitivity to precipitation, blowing snow, and horizontal resolution of the spatial distribution of simulated snow cover," *EGUsphere*, to be published, doi: 10.5194/egusphere-2023-2604.

[43] S. Dingman, *Physical Hydrology*. Long Grove, IL, USA: Waveland Press, 2015.

[44] V. Vionnet et al., "Sub-kilometer precipitation datasets for snowpack and glacier modeling in Alpine terrain," *Front. Earth Sci.*, vol. 7, 2019, Art. no. 182.

[45] H. Rott and T. Nagler, "Capabilities of ERS-1SAR for snow and glacier monitoring in alpine areas," in *Proc. 2nd ERS-1 Symp. ESA SP-361*, 1994, pp. 965–970.

[46] J. Shi and J. Dozier, "Estimation of snow water equivalence using SIR-C/X-SAR. II. inferring snow depth and particle size," *IEEE Trans. Geosci. Remote Sens.*, vol. 38, no. 6, pp. 2475–2488, Nov. 2000.

[47] N. Baghdadi, C. Livingstone, and M. Bernier, "Airborne c-band SAR measurements of wet snow-covered areas," *IEEE Trans. Geosci. Remote Sens.*, vol. 36, no. 6, pp. 1977–1981, Nov. 1998.

[48] M. Tom, R. Aguilar, P. Imhof, S. Leinss, E. Baltsavias, and K. Schindler, "Lake Ice Detection From Sentinel-1 SAR With Deep Learning," in *ISPRS Annals of the Photogrammetry, Remote Sensing and Spatial Information Sciences*, vol. V-32020. Gottingen, Germany: Copernicus, 2020, pp. 409–416.

[49] E. Stonevicius, G. Uselis, and D. Grendaite, "Ice detection with Sentinel-1 SAR backscatter threshold in long sections of temperate climate rivers," *Remote Sens.*, vol. 14, no. 7, Jan. 2022, Art. no. 1627.

[50] J. Kendra, K. Sarabandi, and F. Ulaby, "Radar measurements of snow: Experiment and analysis," *IEEE Trans. Geosci. Remote Sens.*, vol. 36, no. 3, pp. 864–879, May 1998.
[51] C. Vincent et al., "Disparition anticipée du glacier de Saint-Sorlin vers 2050," *La Météorologie*, vol. 2023, no. 121, pp. 39–47, 2023.
[52] M. König, J.-G. Winther, J. Kohler, and F. König, "Two methods for firn-area and mass-balance monitoring of Svalbard glaciers with SAR satellite images," *J. Glaciol.*, vol. 50, no. 168, pp. 116–128, Jan. 2004.

Clémence Turbé received the meteorological engineering degree in 2022 from the École Nationale de la Météorologie, Toulouse, France, and the master's degree in Earth, planetary, and environmental sciences from Université Grenoble Alpes, Grenoble, France, in 2022. She is currently working toward the Ph.D. degree in monitoring snow in mountainous areas using Sentinel-1 imagery with Centre d'Étude de la Neige, CNRM, University of Toulouse, Toulouse, France. Her Ph.D. thesis focuses on the monitoring of wet snow in the French mountains massifs using Sentinel-1 images, by studying the interannual and intermassif variabilities of melting lines, and a comparison with simulations from the Crocus snow pack model.

Fatima Karbou received the Ph.D. degree in physics of remote sensing from the University of Versailles, Saint Quentin en Yvelines, France, in 2004.

She is a Senior Scientist in remote sensing of Earth's surfaces. She spent several years with the CNRM research group on Numerical Weather Prediction (NWP), working on assimilating passive microwave observations over land and sea ice surfaces within global NWP models. She joined the Snow Research Centre in early 2011. Her current research interests include understanding the physics of satellite measurements, monitoring seasonal snow cover in the mountains, mountain lake dynamics, and characterizing some relevant indicators of avalanche activity using Sentinel-1 SAR image time series.

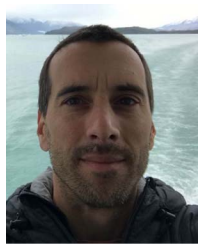

Antoine Rabatel received the Ph.D. degree in Earth, Universe, and environmental sciences from the University Joseph Fourier, Grenoble, France, in 2005.

In 2009, he obtained a permanent position as Researcher with the Laboratory of Glaciology and Environmental Geophysics, Univ. Joseph Fourier–Grenoble, CNRS. Since 2021, he has been a Professor with the Institute for Environmental Geosciences, University Grenoble Alpes, Grenoble, France. He is a Glaciologist. His work is based on field and remote sensing measurements of glacier surface processes. He is coordinating the French Service National d'Observation GLACIOCLIM and the Scientific Expertise Center "Glaciers" from the French National Data Center THEIA which aims at developing and distributing glacier-related products derived from satellite remote sensing observations. His research interests include mountain glaciers processes, long term changes in relation with climate and related impacts on water resources, and hydrological functioning of glacierized catchments.

Isabelle Gouttevin received the Ph.D. degree in Earth, Universe, and environmental sciences from the University of Grenoble, Grenoble, France, in 2012.

Just after graduation, she joined as a permanent Researcher with the Hydrology-Hydraulics Research Unit, IRSTEA (now INRAE), where she focused on different aspects of the hydrological modeling of mesoscale and alpine catchments, including the role of snow and glaciers. During a scientific visit with the CRYOS Lab, EPFL, she, in particular, studied and modeled the snow-forest interactions. In 2018, she joined the Snow Research Center, Grenoble, France, a group of the National Centre for Meteorological Research. As the Head of the Observation team of the Snow Research Center, she promotes synergies between observations of various kinds and their modeling counterparts for a better understanding of the cryosphere and its evolution under climate change. She is currently a Snow Scientist. Her research interests include observing, understanding, and modeling snow and its interactions with the atmosphere, vegetation, and soil in a changing climate. With time, her fields of interest reached to mountain meteorology and the development downscaling and bias correction technics for mountain weather as an upper boundary condition of the snowpack.